ISSN 0018-151X, High Temperature, 2007, Vol. 45, No. 1, pp. 22–31. © Pleiades Publishing, Ltd., 2007.
Original Russian Text © V.G. Asmolov, A.A. Sulatskii, S.V. Beshta, V.S. Granovskii, V.B. Khabenskii, E.V. Krushinov, S.A. Vitol', V.I. Al'myashev, V.V. Gusarov, V.F. Strizhov, 2007, published in Teplofizika Vysokikh Temperatur, Vol. 45, No. 1, 2007, pp. 28–37.

THERMOPHYSICAL PROPERTIES OF MATERIALS

The Interaction of Nuclear Reactor Core Melt with Oxide Sacrificial Material of Localization Device for a Nuclear Power Plant with Water-Moderated Water-Cooled Power Reactor

V. G. Asmolov[a], A. A. Sulatskii[b], S. V. Beshta[b], V. S. Granovskii[b], V. B. Khabenskii[b], E. V. Krushinov[b], S. A. Vitol'[b], V. I. Al'myashev[c], V. V. Gusarov[c], and V. F. Strizhov[d]

[a] *Kurchatov Institute Russian Scientific Center, Moscow, 123182 Russia*

[b] *Aleksandrov Research Institute of Technology, Sosnovyi Bor, Leningrad oblast, 188540 Russia*

[c] *Institute of Silicate Chemistry, Russian Academy of Sciences, St. Petersburg, 199034 Russia*

[d] *Institute of Problems of Safe Development of Nuclear Power Generation, Russian Academy of Sciences, Moscow, 113191 Russia*

Received November 29, 2005

Abstract—The basic results are given of an experimental investigation of the interaction oxide corium melt containing unoxidized zirconium with the sacrificial material of the device for localization of the core melt of a water-moderated water-cooled power reactor (VVER). The mechanism is determined and a model developed of interaction between suboxidized corium melt and sacrificial material.

PACS numbers: 44.35.+C

DOI: 10.1134/S0018151X0701004X

INTRODUCTION

One of the additional protective barriers in the way of propagation of radioactive materials into the environment in the case of heavy accident in a nuclear power plant is provided by an extra-vessel device for localization of melt. For new-generation nuclear power plants with VVER-1000 reactor, a crucible-type catcher has been developed [1]. The corium melt delivered to the catcher is located in a cavity provided with external water cooling and partly filled with so-called sacrificial material (SM).

The purpose of the sacrificial material is to dilute the corium melt delivered from the reactor with a view to reducing its temperature, and to increase the heat-removal surface and reduce the density of oxide melt (the latter provides for the inversion of the oxide and metal layers), as well as to oxidize unoxidized zirconium contained in the delivered melt for reducing the generation of hydrogen in the vapor-zirconium reaction. The SM consists of steel and oxide parts. The composition of oxide SM must contain a component with a high oxidizing resource. We consider only the oxide SM in this study.

In the preliminary stage of selection of SM, integrated experimental and numerical investigations were performed at Aleksandrov Research Institute of Technology, Institute of Silicate Chemistry, Kurchatov Institute, and NPO Luch Scientific-and-Production Association [1]; as a result of these studies, a close-to-equimolar composition was recommended of a mixture of Fe_2O_3 (approximately 65–70% by mass) and Al_2O_3 oxides [2–4]. The experiments [5], performed at the Kurchatov Institute and NPO Luch in the KORPUS and STF facilities under isothermal conditions at temperatures below the corium liquidus temperature with SM of a composition close to that identified above, produced data on the temperature of the beginning of contact melting and on the kinetics and pattern of interaction, as well as on the temperatures of spreading of mixtures of corium with sacrificial material. The experiments resulted in finding the eutectic pattern of the phase diagram of the system, the low (as was expected) eutectic temperature, and high rates of mutual dissolution.

For numerical simulation of the processes occurring in the catcher and for validation of its efficiency, one needs, in particular, to know the kinetics and mechanism of interaction between liquid oxide corium and SM, i.e., at melt temperatures that are much higher than those observed in the experiments of [5]. For this purpose, an experimental investigation was performed of the processes occurring during interaction between suboxidized (containing unoxidized zirconium) corium melt and SM, the mechanism of interaction and the

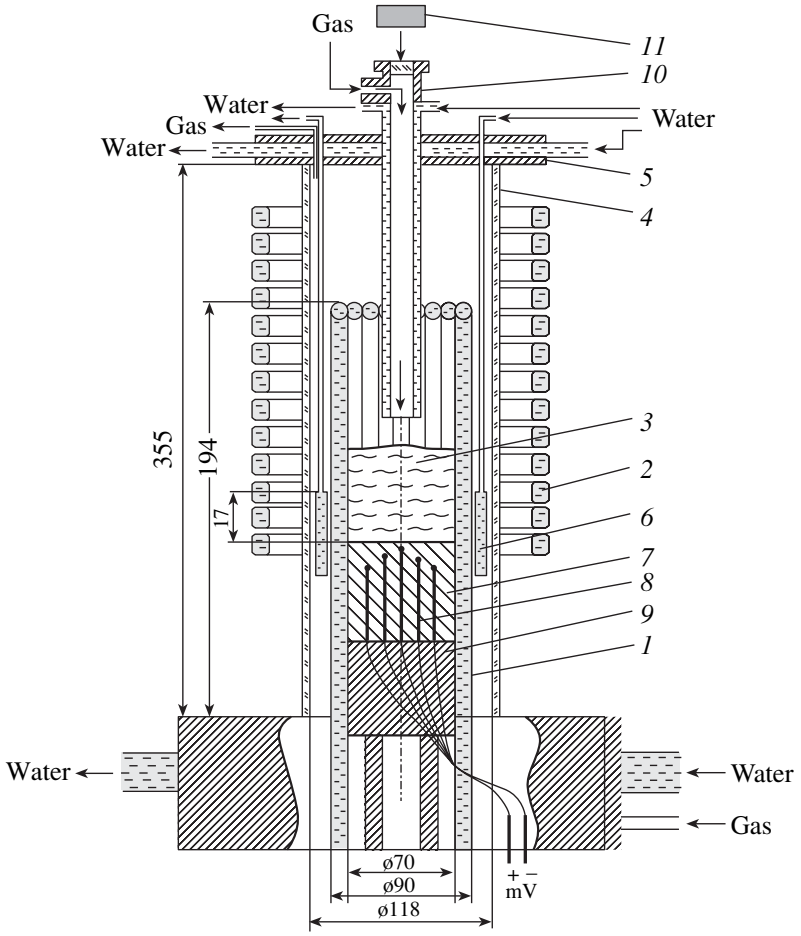

Fig. 1. The induction furnace of Rasplav-3 facility: (*1*) crucible, (*2*) inductor, (*3*) corium melt, (*4*) quartz shell, (*5*) lid, (*6*) electromagnetic screen, (*7*) SM sample, (*8*) thermocouples, (*9*) metal bottom of the crucible, (*10*) pyrometer shaft, (*11*) pyrometer. The dimensions are in mm.

quantitative characteristics of the kinetics of interaction were determined, the experimental data were generalized, and a numerical model was developed.

The experimental investigation involved the use of the technology of induction melting in a cold crucible [6], which served as the basis for development of a series of facilities providing for close-to-real conditions of interaction between corium of different compositions and structural materials.

EXPERIMENT

Experiments with SM were performed in a facility of the Rasplav series, designed for melting suboxidized corium [7]. A schematic view of the facility furnace is given in Fig. 1. The principal components of the furnace include a water-cooled segmented crucible *1* and a water-cooled inductor *2* used for high-frequency heating of corium melt *3*. A quartz shell *4* covered on top by a lid *5* is located between the crucible and inductor. The gap between the quartz shell and inductor accommodates an electromagnetic screen *6* which is one of the means for controlling the heat release in the melt. A cylindrical SM sample *7* provided with thermocouples *8* is placed on a metal bottom *9* of the crucible. The melt temperature is measured by a pyrometer *11* via shaft *10* in the furnace lid. In addition, the pyrometer shaft is used for video recording of the melting process and for delivering argon to the furnace. The basic dimensions of the furnace are given in the figure.

The experiments involved the use of samples with a mass of about 700 g made of ceramic SM elements intended for catchers to be used at Tyanwang nuclear power plant (China) and Kudanculam nuclear power plant (India). The characteristics of SM samples were as follows: composition, % by mass Fe_2O_3 (67.0 ± 1.0), Al_2O_3 (29.0 ± 1.0), SiO_2 (1.9 ± 0.2), Gd_2O_3 (0.14 ± 0.2); porosity (23 ± 2)% by volume; density at 20°C 3600 kg/m^3; thermal conductivity 1.2–1.5 W/(m K).

Figure 2 gives the scheme of temperature measurements of the samples. TC1-TC7 (type K) thermocouples were located in the same axial cross section.

Prior to the beginning of experiments, a charge was placed in the crucible above the SM sample, namely, a

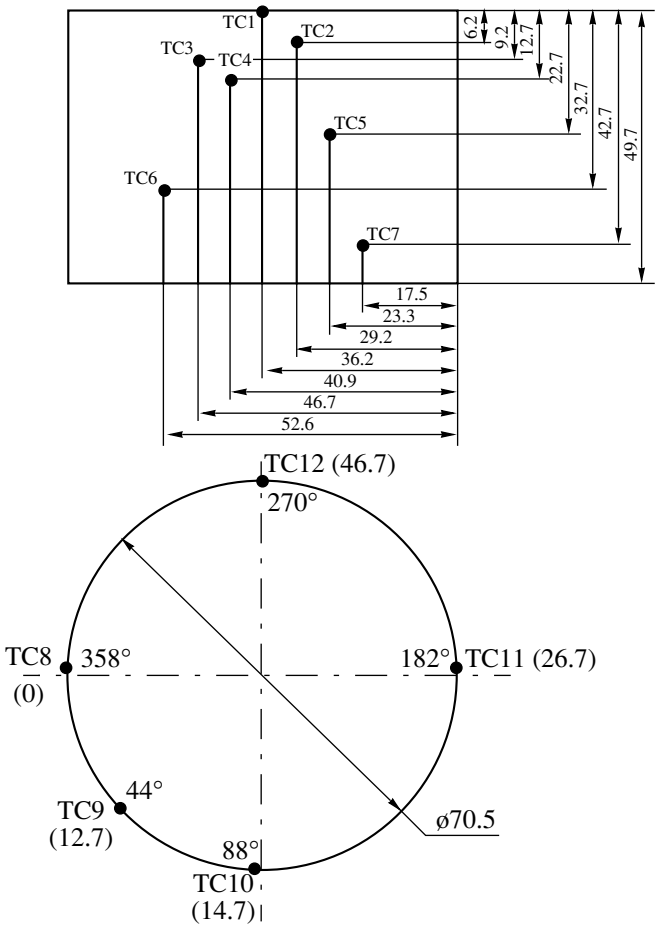

Fig. 2. The scheme of temperature measurements of SM samples: TC1–TC12, thermocouples.

mixture of powders of uranium and zirconium oxides, as well as compact metallic zirconium. The composition of charge in the SACR-8 experiment was as follows: % by mass UO_2 (76), ZrO_2 (9), and Zr (15); the mass of charge was 1404 g. The respective values in the SACR-9 experiment were 74, 20.6% by mass and 1400 g.

This was followed by the heating of the furnace and formation of the melt bath. This process continued for 2200 and 1300 s in the SACR-8 and SACR-9 experiments, respectively.

After the stabilized state of the bath was reached, the pyrometer was used for measuring the surface temperature and sampling the melt. Then, the interaction was initiated by moving the electromagnetic screen below the upper end of the SM sample. In so doing, the surface temperature of the melt was measured continuously; this temperature varied during the period of interaction in the ranges of 2350–2440°C and 2310–2360°C for the SACR-8 and SACR-9 experiments, respectively.

A variation of the form of the surface and of the pattern of melt motion was observed during the interaction between the melt and SM.

The depth of the front of interaction (ablation) of SM was determined by the abrupt increase in the thermocouple readings. It was assumed in what followed that the front of interaction between the melt and SM reached the thermocouple at the instant of time when its temperature increased abruptly to 1400°C. If the thermocouple failed before its readings reached this value, the respective time was determined by extrapolation. Figure 3 gives the readings of thermocouples in the process of interaction using the example of SACR-8 experiment.

After the completion of ablation, the high-frequency heating was discontinued, the melt crystallized, and the ingot was cooled in argon.

RESULTS OF ANALYSIS

The completion of the experiment and disassembly of the crucible were followed by the cutting of the ingot and SM sample and determination of their macrostructure, by the investigation of SM samples by electron microscopy and microanalysis (SEM/EDX), and by elemental analysis of samples of melting products using the method of X-ray diffraction fluorescence analysis.

Figures 4a and 4b give the axial cross sections of ingots. One can see that SM samples *1* interacted with oxide melt *2*. The final form of the interaction surface is close to hemispherical. Note further the large amount of metallic inclusions *3* in crystallized oxide melt.

We will consider the results of SEM/EDX analysis. Figure 5 gives microphotographs of a template located in the region of boundary between oxide ingot and SM sample. The position of this template is marked by a white square in the bottom left corner of Fig. 4a. The table gives the results of SEM/EDX analysis by the basic components for all typical structural constituents of this template. The concentrations of impurity components such as Gd_2O_3, SiO_2, and others are not given in the table.

Several characteristic zones may be identified in the microphotographs of Fig. 5, namely, the zone of thermally stressed state of SM (I) which shows up in the formation of micro- and macrocracks, the zone of plastic behavior and sintering of SM (II), the zone of diffusion of components (III), and the zone of interaction formed by the components of SM and suboxidized corium (IV).

SEM/EDX analysis enables one to identify a number of regularities which are important from the standpoint of developing a model of the process.

1. Clearly defined boundaries are observed between the zone of diffusion of components (III) and the zone of interaction (IV).

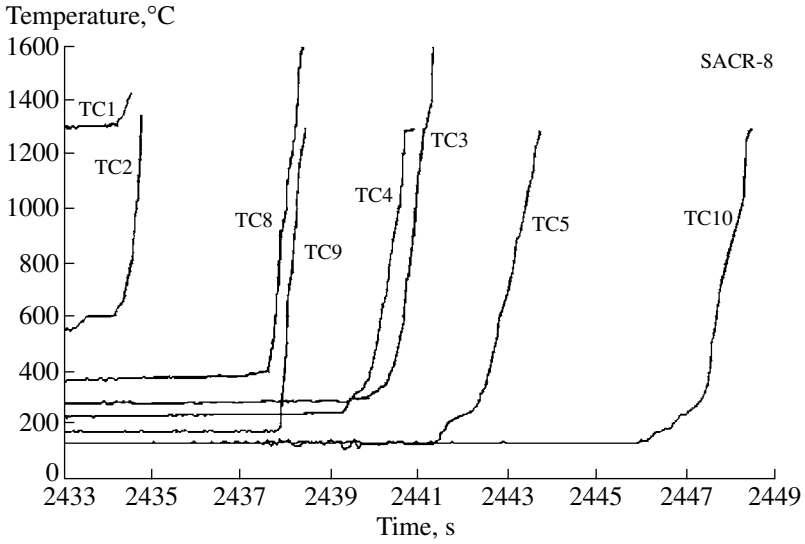

Fig. 3. The readings of thermocouples during SACR-8 experiment.

2. The thickness of the reaction zone (zones III and IV) is small, i.e., approximately 0.6–1.0 mm; within this layer, the oxidation level of iron varies from Fe^{3+} to Fe^0 (metallic iron).

3. The release of oxygen during decomposition of ferric oxide with the formation of numerous pores in zone II (Fig. 5) causes an increase in the thermal resistance of this layer and decelerates the heating of SM.

4. The phase and microstructure homogeneity is observed throughout the height of corium ingot; the ingot consists of solid solutions based on uranic and zirconium oxides and containing impurity amounts of SM components.

5. Macroinclusions of Fe confirm the presence of a stratification dome in the system.

Therefore, the results of analysis of the phases and microstructure of crystallized ingot lead one to conclude that the interaction occurs in a fairly thin layer of melt which directly adjoins the surface of sacrificial material.

ABLATION KINETICS

Based on the foregoing experimental results, the process of propagation of the front of interaction (ablation) may be described as follows.

1. The interaction is initiated on the top surface of SM sample at some initial point (close to the axis) with coordinates (x_0, y_0) at the instant of time τ_0.

2. Ablation occurs at a constant rate W which remains invariant until almost complete exhaustion of non-oxidized zirconium in the melt.

3. The interaction front has a hemispherical shape.

Note that the values of x_0, y_0, τ_0, and W are unknown.

The distance from the ith thermocouple to the initial point is calculated, on the one hand, from the geometric relation

$$R_i = \sqrt{(x_i - x_0)^2 + (y_i - y_0)^2 + z_i^2}, \quad (1)$$

where z_i is Cartesian coordinate reckoned downward from the top surface of SM sample. On the other hand, R_i is the path traveled by the ablation front at the constant rate W in time $(\tau_1 - \tau_0)$,

$$R_i = W(\tau_i - \tau_0). \quad (2)$$

The readings of the peripheral thermocouples TC8–TC12 were not included in analysis, because end effects of the contact between the sample and water-

SEM/EDX data

Zone		UO_2	ZrO_2	Al_2O_3	FeO_x	Fe
		% by mass				
Corium with reaction products	P1	83	15	<1	<1	–
	P2	35	51	5	5	–
	P3	18	15	49	18	–
Metallic inclusions	P4	–	–	–	–	99
	P5	<1	<1	<1	99	–
Zone of interaction	P6	65	12	1	16	–
	P7	33	54	<1	12	–
	P8	<1	<1	1	98	–
	P9	<1	<1	48	51	–
SM	P10	–	< 1	14	85	–
	P11	–	< 1	32	67	–
	P12	–	< 1	87	12	

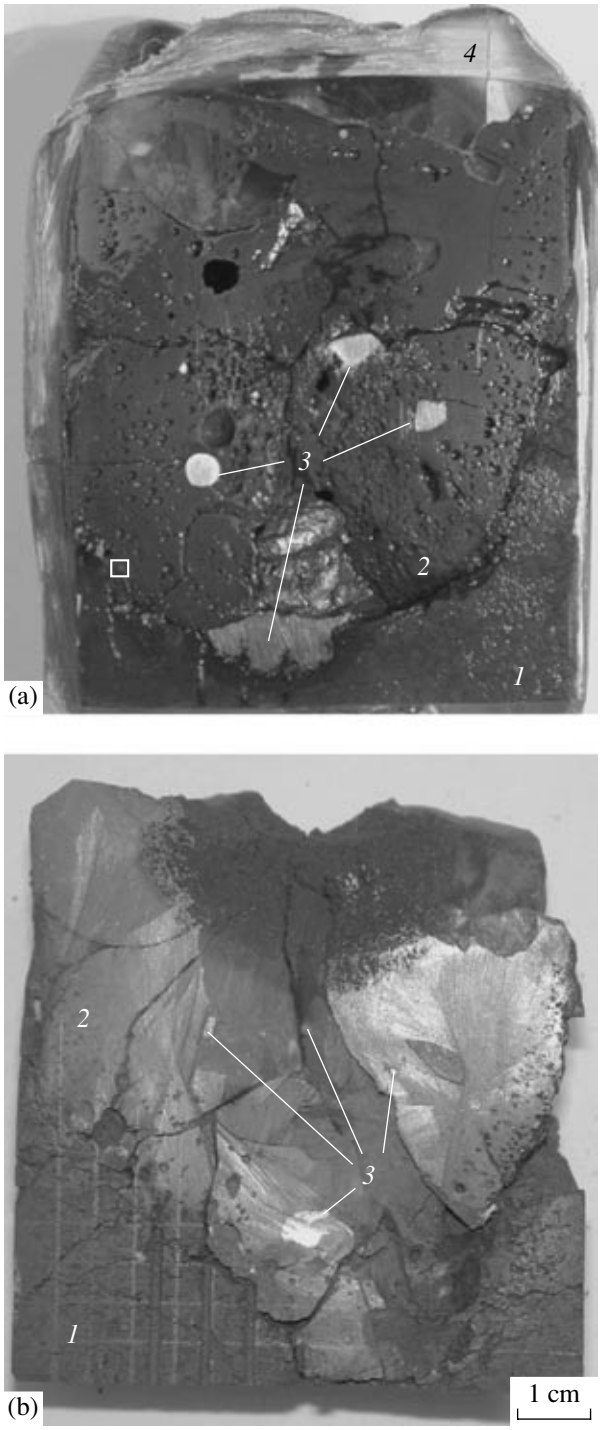

Fig. 4. Axial cross sections of oxide ingots and SM samples: (a) SACR-8 experiment, (b) SACR-9 experiment; (*1*) SM sample, (*2*) oxide melt, (*3*) metallic inclusions, (*4*) epoxy resin.

cooled segments of the crucible showed up in this region. In both experiments, the ablation front did not propagate as far as the location thermocouples TC6 and TC7; therefore, the readings of these latter thermocouples were not used either.

The processing of the experimental results using this procedure produces the values of rate of ablation *W* of 1.94 and 1.75 mm/s for the SACR-8 and SACR-9 experiments, respectively. Therefore, we can round off and agree that the rate of ablation in both experiments amounted to approximately 1.85 (±0.10) mm/s.

Figures 6a and 6b are clearly indicative of the adequate correctness of the assumption of constancy of the rate *W*. The time in the figures is reckoned from the beginning of interaction. One can see in Fig. 6 that all points are well processed using the assumption of constant rate of ablation *W*. The mean absolute deviation of theory from experimental data is 1.3 mm (10% in relative measurement) for SACR-8 experiment and 1mm (15%) for SACR-9 experiment. The maximal deviation for SACR-8 experiment is 1.6 mm or 4% in relative measurement. For SACR-9 experiment, the respective values are 1.8 mm and 35% (TC1 thermocouple, which was the first to operate when the path traveled by the front was still short).

MODEL OF INTERACTION BETWEEN CORIUM AND SM

As was confirmed by the results of analysis, the basic process in the interaction of suboxidized corium melt with SM is the exothermal redox reaction

$$2Fe_2O_3 + 3Zr = 4Fe + 3ZrO_2 \qquad (3)$$

with the energy effect close to 1.8×10^6 J/mol in the temperature range from 1820 to 2700°C.

As the interaction front moves deep into the SM sample, the concentration of Fe_2O_3 in the sample does not vary. One could expect a decay of reaction (3) and a decrease in the rate of ablation with decreasing concentration of one of the reactants, namely, zirconium. However, the experimental results indicate that the rate of ablation does not vary in a wide range of variation of concentration of Zr; therefore, the rate of ablation in this range is limited by the delivery of another component, Fe_2O_3. In so doing, the rate of delivery of Fe_2O_3 is proportional to the rate of ablation of SM. Under these conditions, the observed absence of acceleration of ablation may be due either to the feedback which decelerates the reaction, i.e., to the blocking of the delivery of Fe_2O_3 by the reaction products, or to the peculiar mechanism of redistribution of heat of chemical reaction, or to both these factors.

Considered below is a model of ablation of SM, which is based on the results of analysis of the processes of heat and mass transfer and disregards any mechanisms limiting the delivery of zirconium. The model covers both the region which is independent of the concentration of Zr in corium melt and the region where this concentration is one of the determining factors.

We will now list the assumptions (see Fig. 7) made in developing this model.

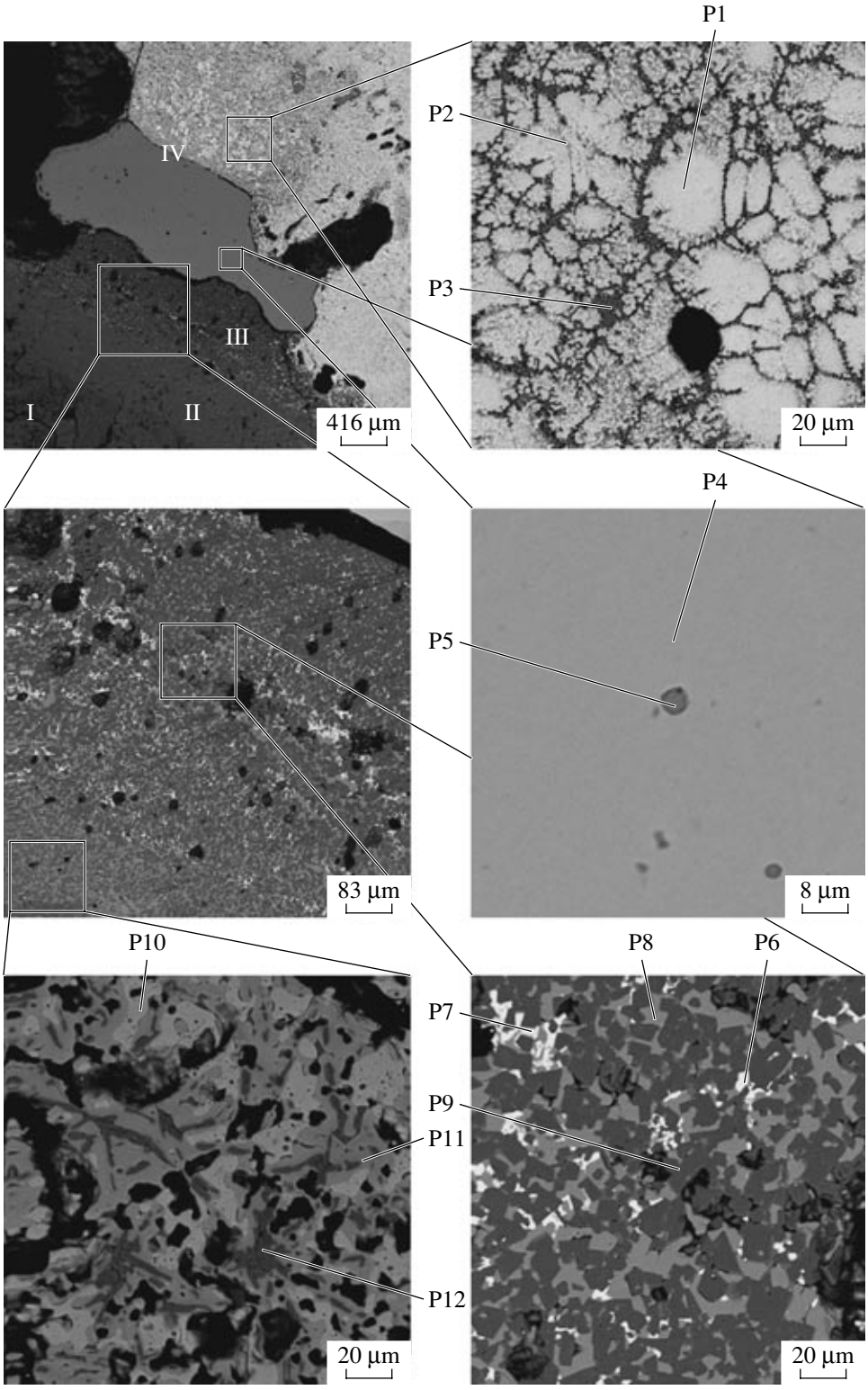

Fig. 5. Microphotographs of a region close to the boundary between corium and SM (SACR-8 experiment).

1. A liquid-phase chemical reaction (3) between ferric oxide and zirconium occurs with an efficiency of 100% during the interaction between melt and sacrificial material.

2. This reaction and corresponding heat release occur in a thin *reaction layer* adjoining the surface of SM.

3. The heat of chemical reaction is spent for heating and melting the SM and for heating the melt compo-

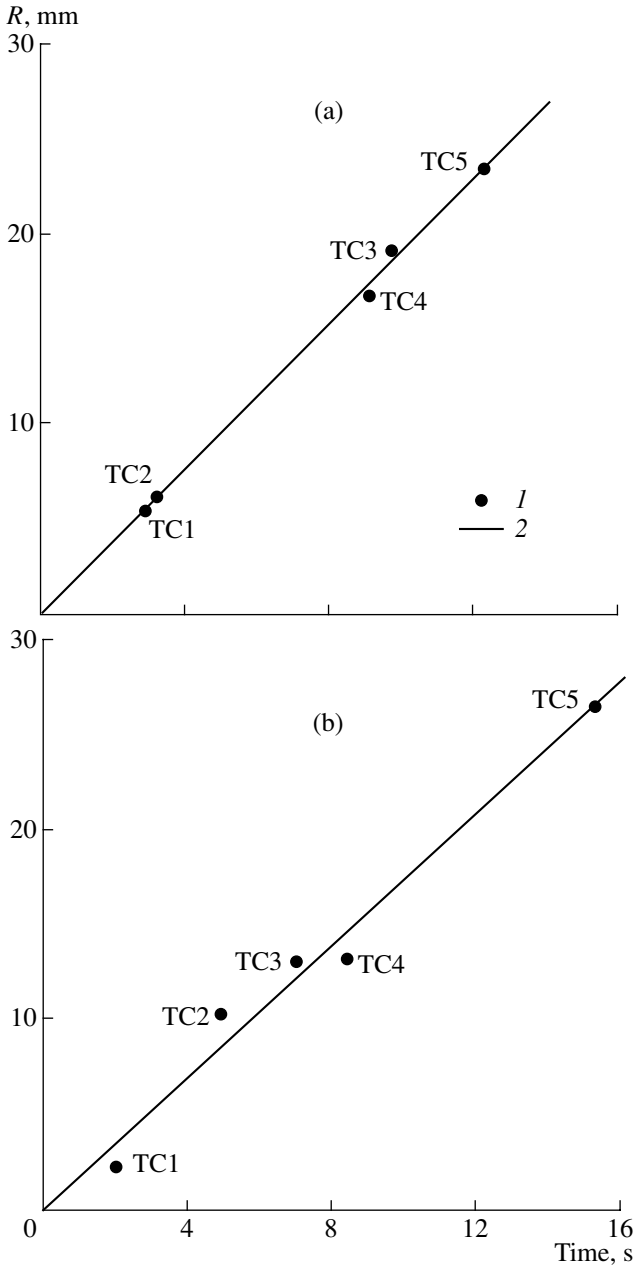

Fig. 6. The propagation of the ablation front: (a) SACR-8 experiment, (b) SACR-9 experiment; (*1*) experiment, (*2*) linear approximation.

nents, which are delivered to the reaction layer, to the temperature of the latter.

4. The heat removal, the delivery of melt components, and the removal of reaction products from the reaction layer are performed owing to natural convection.

5. In view of the high rate of ablation W and low thermal conductivity of SM, the heating of the latter outside of the melting layer is ignored.

We will treat the mass and heat balances in the reaction layer per unit surface of the interaction front.

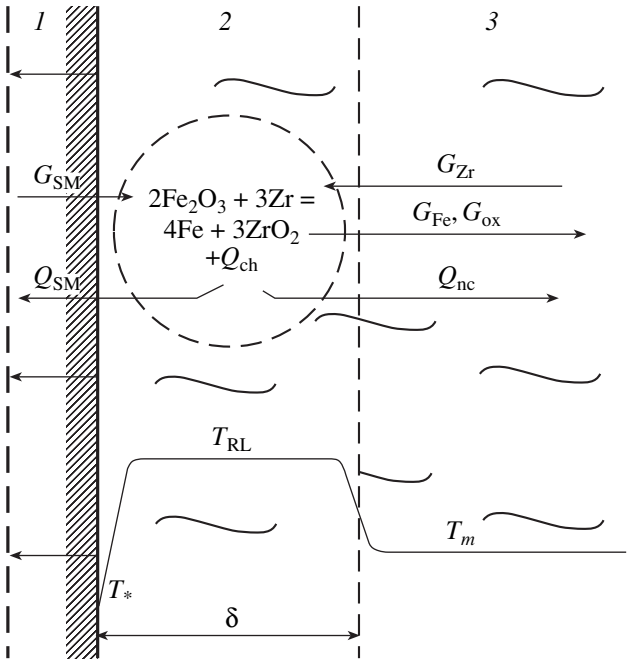

Fig. 7. A model of reaction layer: (*1*) SM, (*2*) reaction layer, (*3*) corium melt.

The mass balance may be written as

$$G_{SM} + G_{Zr} = G_{Fe} + G_{ox}. \quad (4)$$

Here, $G_{SM} = \rho_{SM,s}W$ is the mass flow of SM to the reaction layer;

$$G_{Zr} = \gamma_{Zr}G_{SM} \quad (5)$$

is the mass flow of unoxidized Zr to the reaction layer, which is determined from the stoichiometric relation for reaction (3),

$$\gamma_{Zr} = \frac{3M_{Zr}n_{Fe_2O_3}}{2M_{Fe_2O_3}}, \quad (6)$$

where $n_{Fe_2O_3} = 0.67$ is the mass fraction of ferric oxide in SM;

$$G_{Fe} = \gamma_{Fe}G_{SM} \quad (7)$$

is the mass flow of reaction iron from the reaction layer, which is determined from the stoichiometric relation for reaction (3),

$$\gamma_{Fe} = \frac{2M_{Fe}n_{Fe_2O_3}}{M_{Fe_2O_3}}. \quad (8)$$

and G_{ox} is the mass flow of matter (with the exception of reaction Fe) from the reaction layer to the melt.

Therefore, for G_{ox} from Eq. (4), we derive

$$G_{ox} = G_{SM} + G_{Zr} - G_{Fe} = (1 + \gamma_{Zr} - \gamma_{Fe})\rho_{SM,s}W. \quad (9)$$

The heat balance has the form

$$Q_{ch} + h_{SM}(T_{SM})G_{SM} + h_{Zr}(T_m)G_{Zr} = Q_{SM} + Q_{nc} + h_{ox}(T_{RL})G_{ox} + h_{Fe}(T_{RL})G_{Fe}. \quad (10)$$

In Eq. (10),

$$Q_{ch} = r_{ch}G_{SM} = r_{ch}\rho_{SM,s}W \quad (11)$$

is the heat release due to chemical reaction;

$$h_{SM}(T_{SM})G_{SM} = h_{SM}(T_{SM})\rho_{SM,s}W \quad (12)$$

is the delivery of heat with the mass flow of SM in so doing, $T_{SM} = T_*$ (the SM surface temperature T_* is close to the temperature of the eutectic of the system of components involved in the interaction and is estimated to be 1400°C);

$$h_{Zr}(T_m)G_{Zr} = h_{Zr}(T_m)\gamma_{Zr}\rho_{SM,s}W \quad (13)$$

is the delivery of heat with the flow of unoxidized Zr from the melt at temperature T_m;

$$Q_{SM} = \alpha_{RL}(T_{RL} - T_*) = r_{SM}\rho_{SM,s}W \quad (14)$$

is the heat flux which is delivered to the SM surface from the reaction layer and, by virtue of low thermal conductivity of SM and high rate of interaction, is fully spent for the ablation of SM;

$$r_{SM} = r_m n_{Fe_2O_3} + c_{SM,s}(T_* - T_{SM,0}) \quad (15)$$

is the melting heat of SM in view of additional heating of SM from the initial temperature $T_{SM,0} \approx 20$°C to T_*, and r_m is the melting heat of ferric oxide (Al_2O_3, which is present in the composition of SM, at T_* stays in the solid phase);

$Q_{nc} = \alpha_{nc}(T_{RL} - T_m)$ is the heat removal from the reaction layer by natural convection to the melt. Here,

$$\alpha_{nc} = C_{nc}\left[\frac{c_1(\rho\lambda)^2\beta(T_{RL} - T_m)g}{\mu}\right]^{1/3} \quad (16)$$

is the coefficient of natural-convection heat transfer from the reaction layer to the melt [8], where the proportionality factor C_{nc} is 0.15 for a vertical surface. We assume that, for a hemispherical surface, $C_{nc} = 0.15$, and the physical properties used in relation (16) relate to oxide melt [9];

$$h_{ox}(T_{RL})G_{ox} = h_{ox}(T_{RL})(1 + \gamma_{Zr} - \gamma_{Fe})\rho_{SM,s}W \quad (17)$$

is the carry-over of heat with the mass flow of oxides from the reaction layer to the melt; and

$$h_{Fe}(T_{RL})G_{Fe} = h_{Fe}(T_{RL})\gamma_{Fe}\rho_{SM,s}W \quad (18)$$

is the carry-over of heat with the mass flow of Fe from the reaction layer.

Therefore, expressions (9)–(18) represent a set of equations for two unknowns, namely, α_{RL} and T_{RL}, because the rate of ablation W is determined experimentally.

We make the following assumptions in determining the model of heat transfer between the reaction layer and SM surface:

the heat transfer exhibits a natural-convection pattern;

the melt motion in the reaction layer proceeds in the turbulent mode, which enables one to eliminate the dependence on the linear dimensions of the system, i.e., on the reaction layer thickness (δ);

the determining factor of natural convection is the heat release in the reaction layer due to chemical reaction.

In view of the foregoing, the heat transfer coefficient α_{RL} may be written as

$$\alpha_{RL} = C_{RL}\frac{\lambda}{\delta}\mathrm{Ra}_q^m. \quad (19)$$

Here, C_{RL} is the coefficient determined by the processing of experimental data;

$$\mathrm{Ra}_q = \frac{c_1\rho^2 q_v \beta g \delta^5}{\mu\lambda^2} \quad (20)$$

is the modified Rayleigh number used in problems in natural convection with volumetric energy release; m is the exponent selected such as to eliminate the dependence of α_{RL} on δ; the physical properties used in relation (20), as well as in (16), are the properties of oxide melt; and

$$q_v = r_{ch}\rho_{SM,s}W/\delta \quad (21)$$

is the specific energy release per unit volume due to chemical reaction.

We substitute Eq. (21) into (20) to derive

$$\mathrm{Ra}_q = \frac{c_1\rho^2 r_{ch}\rho_{SM,s}W\beta g\delta^4}{\mu\lambda^2}, \quad (22)$$

whence follows, in view of the assumption of α_{RL} independence of the reaction layer thickness (δ), that $m = 1/4$; for the heat transfer coefficient α_{RL}, we derive

$$a_{RL} = C_{RL}\left[\frac{c_1(\rho\lambda)^2 r_{ch}\rho_{SM,s}W\beta g}{\mu}\right]^{1/4}. \quad (23)$$

We use Eqs. (23) and (14) to find C_{RL},

$$C_{RL} = \frac{r_{SM}(\rho_{SM,s}W)^{3/4}\mu^{1/4}}{[c_1(\rho\lambda)^2 r_{ch}\beta g]^{1/4}(T_{RL} - T_*)}, \quad (24)$$

where W is known from experiment, and T_{RL} is calculated using the set of equations (9)–(18). The melt bath temperature T_m was taken to be 2360 and 2460°C for SACR-8 and SACR-9 tests, respectively. The calculations by the described procedure produce a value of T_{RL} of 2650°C for the conditions of both experiments, and the coefficient C_{RL} is equal to 0.31.

Therefore, the expression for the coefficient of heat transfer between the reaction layer and SM surface takes the form

$$\alpha_{RL} = 0.31\left[\frac{c_1(\rho\lambda)^2 r_{ch}\rho_{SM,s}W\beta g}{\mu}\right]^{1/4}. \quad (25)$$

Note that, in spite of significant energy release associated with the heat of exothermal reaction of oxidation of Zr, no significant increase in the melt temperature occurs in the SACR-8 and SACR-9 experiments: during interaction, this temperature increases by not more than 50°C. As was demonstrated above, a significant increase in temperature is observed only within the reaction layer.

After expression (25) is derived, the set of equations (9)–(18) becomes completely closed. Given the parameters of the coolant (its temperature T_m and physical properties), one can determine the reaction layer temperature T_{RL} and, what is most important, the rate of ablation W.

It is necessary to specify the range of validity of the model of interaction between SM and oxide corium melt, which was discussed in this section, as regards the important process parameter such as the concentration of unoxidized Zr in the melt. All of the foregoing analysis holds for the stage of the process in which Zr is present in excess and the rate of the process is limited by the delivery of ferric oxide from SM to the reaction layer. In the course of oxidation reaction, the concentration of Zr decreases, and an instant must inevitably come when this component will be in deficit and it will be its concentration in the melt that will limit the rate of the process. In so doing, the reaction rate will be defined by convective transfer of Zr to the reaction layer from the melt.

In the general case, the convective flow of a component is proportional to the difference between its concentrations in the bulk and at the surface. Under the conditions being considered, the concentration at the surface is approximately zero, i.e., the mass flow of Zr to the reaction layer is proportional to n_{Zr} in the bulk. Then the velocity of motion of the surface of interaction in the general case may be calculated as follows:

$$W = W_\infty \min(1; n_{Zr}/n_{Zr,cr}). \quad (26)$$

Here, W_∞ corresponds to a quantity which is self-similar relative to concentration of Zr in the melt and is determined by the foregoing model, and $n_{Zr,cr}$ is some critical value of mass concentration of Zr in the melt. Below this value, we have the mode of limitation of the rate of the process by the content of zirconium in the melt.

The boundary value of $n_{Zr,cr}$ cannot be determined in the performed experiments, because their very procedure was specialized, tuned to the investigation of interaction between SM and highly under-oxidized corium. The minimal calculated value of mass concentration of Zr in the melt (≈0.4% by mass) was obtained in the SACR-9 experiment at the instant of time when the interaction front reached the TC5 thermocouple. However, even with this low concentration of zirconium, the rate of ablation remained approximately constant, i.e., Zr was present in the melt in sufficient amount. Therefore, one can only state with any assurance that $n_{Zr,cr} < 0.4\%$ by mass.

Therefore, the suggested model of interaction makes it possible to calculate the processes in the device for the localization of melt, which occurred in the zone of location of suboxidized oxide corium, with transition to the calculation of interaction between fully oxidized corium and SM.

In the calculations of the formation of the melt bath in the catcher, rather than reducing to zero the velocity of motion of interaction front with n_{Zr} decreasing below $n_{Zr,cr}$ (this is specific only to the experiments considered by us), it should be reduced to some value corresponding to regular natural-convective heat transfer of the melt of fully oxidized corium with SM (W_{nc}),

$$W = (W_\infty - W_{nc})\min(1; n_{Zr}/n_{Zr,cr}) + W_{nc}. \quad (27)$$

So, the suggested model of interaction enables one to calculate the processes in the device for the localization of melt, which occurred in the zone of location of suboxidized oxide corium, with transition to the calculation of interaction between fully oxidized corium and SM.

CONCLUSIONS

The experimental investigations described in this paper led to the following conclusions.

1. The basic chemical reaction is the oxidation of zirconium by ferric oxide (III) with the formation of metallic iron.

2. The resultant oxide melt exhibits a homogeneous structure. The stratification is observed only between oxides and metal.

3. The velocity of motion of interaction front is approximately constant for the experimental conditions, 1.85 (±0.10) mm/s, and independent of the concentration of zirconium if the latter concentration exceeds 0.4% by mass.

A model of interaction has been developed, which generalizes well the obtained experimental data and is used in the CORCAT codes used for the simulation of the formation of the melt bath in localization devices of the crucible type for nuclear power plants with VVER-1000.

ACKNOWLEDGMENTS

We are grateful to Dr. S. Hellmann (Framatome ANP) for fruitful discussions and valuable recommendations.

This study was supported by the Russian Foundation for Basic Research (project no. 06-08-00258-a).

Notation: C, dimensionless coefficient; c, specific heat capacity in J/(kg K); G, mass flow in kg/(m^2 s); g, acceleration of gravity in m/s^2; h, specific enthalpy in J/kg; M, molecular mass in kg/mol; m, exponent; n, concentration in % by mass; Q, heat flux in W/m^2; q_v, bulk density of heat release in W/m^3; R, distance between the point of beginning of interaction and the hot junction of thermocouple in m; r, latent heat of melting in J/kg; r_{ch}, heat of chemical reaction in J/kg; Ra_q, modified Rayleigh number; T, temperature in K; T_*, SM surface temperature in K; W, rate of ablation in m/s; x, y, and z, Cartesian coordinates in m; α, heat transfer coefficient in W/(m^2 K); β, temperature coefficient of volumetric expansion, 1/K; γ, dimensionless coefficient; δ, thickness of the reaction layer in m; λ, thermal conductivity in W/(m K); μ, dynamic viscosity in Pa s; ρ, density in kg/m^3; τ, time in s.

Subscripts: 0, initial; boil, boiling; ch, chemical; cr, critical; Fe, iron; Fe_2O_3, ferric oxide (III); i, thermocouple number; l, liquid; m, melt or melting; nc, natural (free) convection; RL, reaction layer; ox, oxide; s, solid; sf, surface; SM, sacrificial material; Zr, zirconium.

Abbreviations: SEM/EDX, electron microscopy and microanalysis; TC, thermocouple; VVER, water-moderated water-cooled power reactor; SM, sacrificial material.

REFERENCES

1. Asmolov, V.G., Bechta, S.V., Berkovich, V.M. et al., VVER-1000 Reactor Core Melt Catcher of Cold Crucible Type, in *Proc. Int. Congress on Advances in Nuclear Power Plants (ICAPP 05)*, Seoul, 2005, p. 5238.
2. Gusarov, V.V., Khabenskii, V.B., Beshta, S.V. et al., RF Patent 2 191 436, 2002.
3. Gusarov, V.V., Al'myashev, V.I., Khabenskii, V.B. et al., RF Patent 2 192 053, 2002.
4. Gusarov, V.V., Al'myashev, V.I., Khabenskii, V.B. et al., RF Patent 2 212 719, 2003.
5. Asmolov, V.G., Zagryazkin, V.N., Isaev, I.F. et al., *At. Energ.*, 2002, vol. 92, issue 1, p. 7.
6. Petrov, Yu.B., *Induktsionnaya plavka okislov* (Induction Melting of Oxides), Leningrad: Energoatomizdat, 1983.
7. Bechta, S.V., Khabensky, V.B., Granovsky, V.S. et al., New Experimental Results on the Interaction of Molten Corium with Reactor Vessel Steel, in *Proc. Int. Congress on Advances in Nuclear Power Plants (ICAPP 04)*, Pittsburgh, 2004, p. 4114.
8. *Teoreticheskie osnovy teplotekhniki. Teplotekhnicheskii eksperiment. Spravochnik* (Theoretical Principles of Heat Engineering. Heat-Engineering Experiment: A Reference Book), Grigor'ev, V.A. and Zorin, V.M., Eds., Moscow: Energoatomizdat, 1988.
9. *SCDAP/RELAP5/MOD2. Code Manual, Vol. 4: MATPRO-A Library of Materials Properties for Light-Water-Reactor Accident Analysis*, Hohost, J.K., Ed., NUREG/CR-5273, EGG-2555, 1990.